Simulating Energy Transfer in Molecular Systems with Digital Quantum Computers

Chee-Kong Lee*

Tencent America, Palo Alto, CA 94306, United States

Jonathan Wei Zhong Lau†

Centre for Quantum Technologies, National University of Singapore, 117543, Singapore

Liang Shi‡

Chemistry and Chemical Biology, University of California,

Merced, California 95343, United States

Leong Chuan Kwek§

Centre for Quantum Technologies, National University of Singapore, 117543, Singapore

National Institute of Education, Nanyang Technological University,

1 Nanyang Walk, Singapore 637616 and

MajuLab, CNRS-UNS-NUS-NTU International Joint Research Unit, UMI 3654, Singapore

1

Abstract

Quantum computers have the potential to simulate chemical systems beyond the capability of classical computers. Recent developments in hybrid quantum-classical approaches enable the determinations of the ground or low energy states of molecular systems. Here, we extend near-term quantum simulations of chemistry to time-dependent processes by simulating energy transfer in organic semiconducting molecules. We developed a multi-scale modeling workflow that combines conventional molecular dynamics and quantum chemistry simulations with hybrid variational quantum algorithm to compute the exciton dynamics of an N-molecule system, encoded in $\log_2(N)$ qubits. Our numerical examples demonstrate the feasibility of this approach, and simulations on IBM Q devices capture the qualitative behaviors of exciton dynamics but with considerable errors. We present an error mitigation technique that combines experimental results from the variational and Trotter algorithms, and obtain significantly improved quantum dynamics. Our approach opens up new opportunities for modeling quantum dynamics in chemical, biological and material systems with quantum computers.

* Electronic address: cheekonglee@tencent.com

† Electronic address: e0032323@u.nus.edu

‡ Electronic address: lshi4@ucmerced.edu

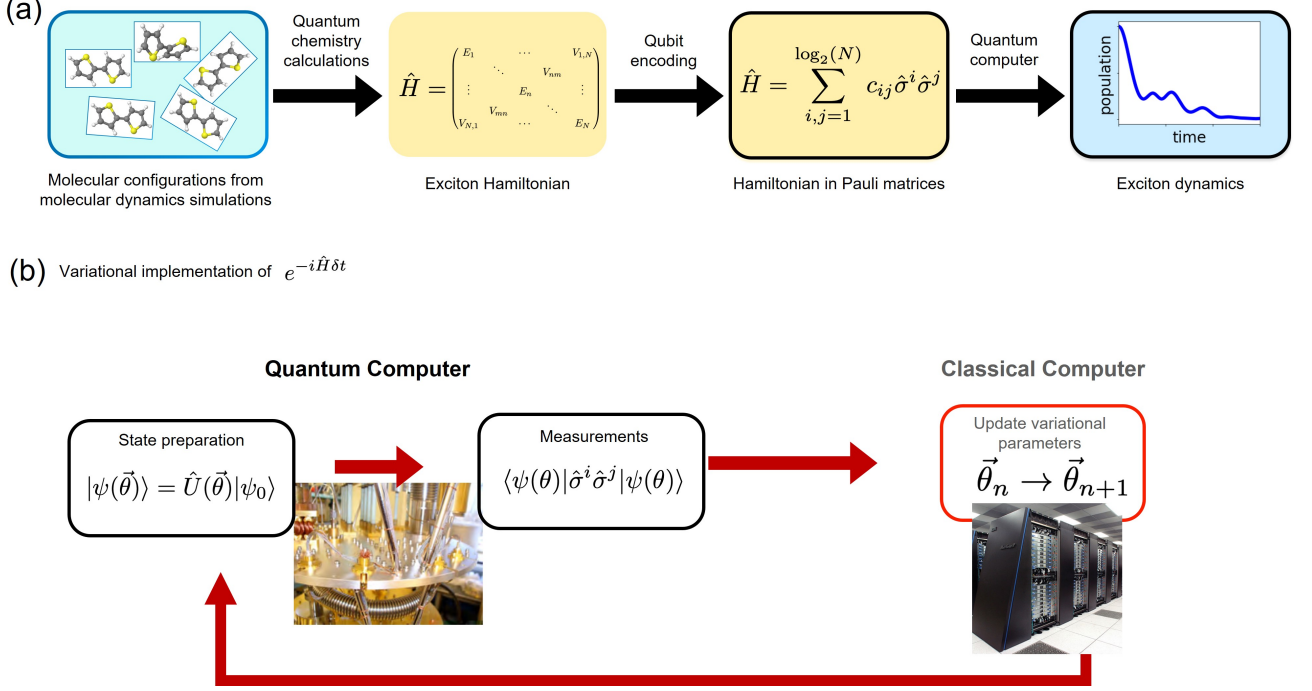§ Electronic address: cqtklc@nus.edu.sg

(a)

Molecular configurations from molecular dynamics simulations

Quantum chemistry calculations

Exciton Hamiltonian

$$\hat{H} = \begin{pmatrix} E_1 & \cdots & & V_{1,N} \\ & \ddots & & V_{nm} \\ \vdots & & E_n & \vdots \\ & V_{mn} & \ddots & \\ V_{N,1} & \cdots & & E_N \end{pmatrix}$$

Qubit encoding

Hamiltonian in Pauli matrices

$$\hat{H} = \sum_{i,j=1}^{\log_2(N)} c_{ij} \hat{\sigma}^i \hat{\sigma}^j$$

Quantum computer

Exciton dynamics

(b) Variational implementation of $e^{-i\hat{H}\delta t}$

Quantum Computer

State preparation

$$|\psi(\vec{\theta})\rangle = \hat{U}(\vec{\theta})|\psi_0\rangle$$

Measurements

$$\langle\psi(\theta)|\hat{\sigma}^i\hat{\sigma}^j|\psi(\theta)\rangle$$

Classical Computer

Update variational parameters

$$\vec{\theta}_n \rightarrow \vec{\theta}_{n+1}$$

FIG. 1: (a) A schematic of the setup in this work. The molecular configurations are obtained from molecular dynamics simulations. From these molecular configurations, quantum chemistry calculations are utilized to obtain the exciton Hamiltonian. An N-molecule exciton Hamiltonian is then encoded in $\log_2(N)$ qubits with a binary encoding scheme. Finally we simulate the quantum dynamics of the exciton system with a digital quantum computer. (b) A variational quantum algorithm is used to simulate the time evolution of excitonic system. The wavefunction at time t is represented by a parametrized circuit ansatz, $|\Psi(t)\rangle \approx \left|\psi(\vec{\theta}(t))\right\rangle$. The variational parameters are updated iteratively with a classical computer based on the measurement outputs from the quantum computer. The updated parameters are then sent to quantum computer for preparation of a new quantum state.

I. INTRODUCTION

Quantum simulation of chemical systems is one of the most promising and anticipated applications for quantum computers[1–6]. Classical simulation of quantum systems becomes exponentially complex with an increasing number of degrees of freedom. Even for a modest-sized molecule of tens of atoms, accurate simulation on a classical computer remains challenging. A quantum computer reputedly allows us to tackle some of these classically

intractable computational problems more efficiently. Such computations enable us to design better compounds for chemistry, materials science and biology. In recent years, there are numerous experimental and theoretical works that focus on the determination of the ground or low-energy eigenstates of molecular systems with near-term digital quantum computers [7–21]. However, many phenomena in chemistry are dynamical and require a time-dependent solution, e.g. energy transfer, chemical reactions, and spectroscopy [22–24]. Understanding these processes would therefore require the simulation of the time evolution of the relevant quantum systems. This task is typically more difficult than the computation of static ground state properties since it often involves the participation of all quantum states. Despite its relevance and importance, research on simulating time-dependent processes in chemical systems with noisy intermediate-scale quantum (NISQ) devices remains limited [25–27].

While there are a number of quantum algorithms to simulate the dynamics of quantum many-body systems, such as those based on Trotterization [28], linear combination of unitaries [29], quantum signal processing [30] and qubitization [31], these algorithms require long circuit depth and are therefore not suitable for NISQ devices due to their intrinsic errors. Hence we adopt a variational quantum algorithm (VQA) based on the McLachlan's principle to simulate these time-dependent processes in chemical systems [32–34]. Within the VQA, the time-dependent wavefunction is represented by a parametrized quantum state $\left|\psi(\vec{\theta})\right\rangle$ that can be prepared efficiently in a quantum computer. The variational parameters are updated iteratively by the classical computer via the optimization of the time-dependent Schrodinger equation. As a result of the integration with classical computer, the VQA algorithm can be implemented with quantum circuits of much shallower depth compared with other conventional algorithms for Hamiltonian simulations.

For noisy quantum systems, fault-tolerant quantum computing using quantum error correction codes has been proposed as a means to assuage the effects of errors. Quantum information is encoded in logical qubits each comprising of many physical qubits, and the computation error can be reduced to arbitrarily small value provided that the error of each physical qubit is smaller than a certain threshold value. For NISQ devices, the number of physical qubits is likely to be restricted. Thus before the realization of quantum error correction, error mitigation in NISQ devices has been proposed as an alternative to fault-tolerant quantum computing. Several error mitigation techniques have since been developed, e.g. error extrapolation [32], quasi-probability method [35], quantum subspace expansion [36]

and machine learning [37]. In this work, we demonstrate a new error mitigation method for quantum dynamics by combining the experimental results from the VQA and a Trotterization scheme. This error mitigation method is motivated by the intuition that Trotterized quantum simulation is accurate in short time even in noisy quantum circuits, therefore useful information can be extracted from the short-time Trotter dynamics to mitigate errors in the VQA. We show that such error mitigation method significantly improves the accuracy of quantum dynamics simulation by performing experiments in IBM quantum computers. To the best of our knowledge, it is the first demonstration of performing error mitigation by combining the results from two different algorithms, namely a hybrid variational algorithm and a fault tolerant algorithm.

We demonstrate the feasibility of using a digital quantum computers to simulate quantum dynamics in chemical systems by studying the energy transfer process. To be exact, we consider excitonic energy transfer in organic semiconducting molecules. Exciton is a quasi-particle excitation consisting of a bound pair of electron and hole that mediates the energy transport in a wide range of systems ranging from photosynthetic light harvesting systems, organic light-emitting diodes (OLEDs) to organic photovoltaics (OPVs) [38–40]. Understanding exciton transfer in experimentally relevant systems is thus vital for various technological applications, e.g. designing more efficient and robust OPVs and OLEDs. However, quantum mechanical simulation of the exciton dynamics in molecular systems can be challenging due to the presence of disorder (both static and dynamical) and the large number of excitonic sub-units involved. Quantum computers could potentially overcome these computational challenges.

We aim to study chemical systems with direct relevance in chemistry and practical applications. Thus we choose bi-thiophene (T2) as our test system. T2 molecule represents the minimum model within the family of thiophene-based polymers, one of the most studied semiconducting organic materials, and it has important applications in thin film technology, such as field-effect transistors [41]. To include the effects of complex environment on quantum dynamics, we employ multi-scale modelling by performing molecular dynamics (MD) and quantum chemistry calculations to extract the input Hamiltonian for our quantum computer simulations. The setup of this work is shown in Fig. 1a. We first perform classical MD simulation to obtain the molecular configurations of T2 molecules. For each MD snapshot, quantum chemistry calculations are used to obtain the instantaneous single-molecule

excited-state energies, E_i, and inter-molecular couplings, V_{ij}. Once all the energies and couplings along the MD trajectory are computed, the time-dependent exciton Hamiltonian can then be constructed. The detail of the exciton model is described in Sec. II A. In Sec. II B, we show that the exciton Hamiltonian of N molecules can be encoded into $\log_2(N)$ qubits using a binary encoding scheme. With this efficient encoding methods, three-dimensional systems of practical interest that consist of millions of molecules/sub-units can be encoded in just tens of qubits.

The excitonic wavefunction is then evolved according to the encoded Hamiltonian using the VQA algorithm, illustrated in Fig. 1b. We first present the numerical results of exciton dynamics in a molecular crystal of T2 molecules in Section II D, and observe good agreement between VQA results and exact calculations. We assess the capability of current quantum devices in simulating exciton dynamics in Section II D by implementing the VQA on IBM Q quantum devices. Despite that only short circuit depth is needed, the VQA only qualitatively captures the behaviors of the true exciton dynamics, with some considerable quantitative discrepancy. Finally in II F we discuss the source of errors and propose a new error mitigation technique by combining the VQA result with that from a standard Trotter scheme. Motivated by the insight that the short-time dynamics from the Trotter method is accurate, we advocate correcting the VQA simulation results with the information extracted from the short-time Trotter dynamics. We demonstrate that this error-mitigation technique significantly improves the accuracy of the VQA simulation.

II.   RESULTS

A.   Exciton Hamiltonian

We adopt an *ab-initio* exciton model where the electronic excitation in a multi-chromophoric system is expressed in a basis of localized Frenkel excitations with input from MD simulation and quantum chemical calculations. [42, 43] The resulting (Frenkel) exciton Hamiltonian describes a system of N excitable subunits (also called sites or chromophores) that can each host a localized exciton. The ground electronic state of the system is denoted as $|0\rangle$, the wavefunction for the localized exciton is $|m\rangle = \hat{e}_m^\dagger |0\rangle$, where the creation operator $\hat{e}_m^\dagger$ generates an exciton localized on the m-th site. The form of the creation operator

6

depends on the selected excited-state electronic-structure method. In the basis of these wavefunctions, the exciton Hamiltonian is written as

$$\hat{H}_{\text{exciton}} = \sum_m E_m(t) \left| m \right\rangle \left\langle m \right| + \sum_{m \neq n} V_{mn}(t) \left| m \right\rangle \left\langle n \right|, \tag{1}$$

where E_m is the excitation energy of molecule m and V_{mn} is the coupling between local excitations on molecules m and n.

The time dependence of the excitation energies and excitonic couplings in the exciton Hamiltonian originates from the modulation of the electronic excitation by nuclear motion, sometimes termed exciton-phonon couplings, which heavily influences exciton transport [44–46]. There are multiple approaches to model the exciton-phonon couplings, e.g. phenomenologically through Gaussian white noise or a bath of quantum harmonic oscillators. Here, we adopt an all-atom approach by combining classical MD simulations and time-dependent density functional theory (TDDFT) quantum chemistry calculations. In this approach, the time-dependent fluctuation of the exciton Hamiltonian is provided by fully atomistic simulations without resort to phenomenological models. The details of the MD and TDDFT calculations, and the construction of the exciton Hamiltonian can be found in the Methods section.

B. Mapping to qubits

To simulate exciton dynamics with a digital quantum computer, we need to map the exciton Hamiltonian in Eq. 1 onto qubits. For simplicity, we use a standard binary encoding scheme in which the quantum states of an N-site excitonic model can be encoded in the quantum states of $L = \log_2(N)$ qubits. The binary encoding method has previously been used to encode bosonic degrees of freedom with qubits in the calculation of vibrational spectroscopy [47–49]. Within the binary encoding scheme, an excitonic state $\left| m \right\rangle$ is represented by

$$\left| m \right\rangle = \left| \boldsymbol{x} \right\rangle = \left| x_1 \right\rangle \otimes \left| x_2 \right\rangle \otimes ... \left| x_L \right\rangle, \tag{2}$$

where where the subscript denotes the qubit number, $m = x_1 2^0 + x_2 2^1 ... + x_L 2^{L-1}$ and x_i can be 0 or 1.

7

We note that each operator, $|m\rangle \langle n|$, on the right-hand side (RHS) of Eq. 1 can be mapped to qubit representation using the relation in Eq. 2

$$|m\rangle \langle n| = |\boldsymbol{x}\rangle \langle \boldsymbol{x}'| = |x_1\rangle \langle x_1'| \otimes |x_2\rangle \langle x_2'| \otimes ... \otimes |x_L\rangle \langle x_L'| . \tag{3}$$

Each single qubit operator on the RHS of Eq. 3 can then be expressed in terms of Pauli and identity matrices using the following identities

$$|0\rangle \langle 1| = \frac{1}{2}(\hat{\sigma}_x + i\hat{\sigma}_y) \ ; \ |1\rangle \langle 0| = \frac{1}{2}(\hat{\sigma}_x - i\hat{\sigma}_y);$$

$$|0\rangle \langle 0| = \frac{1}{2}(I + \hat{\sigma}_z) \ ; \ |1\rangle \langle 1| = \frac{1}{2}(I - \hat{\sigma}_z). \tag{4}$$

It is worth noting that the resulting Hamiltonian after encoding can be complicated since it could contain many-body interactions encompassing all L qubits. For example, a 4-site exciton Hamiltonian can be mapped into the following two-qubit Hamiltonian (up to an identity matrix)

$$
\begin{aligned}
H &= \frac{1}{4}(E_1 + E_2 - E_3 - E_4)\hat{\sigma}_z^1 + \frac{1}{4}(E_1 - E_2 + E_3 - E_4)\hat{\sigma}_z^2 \\
&+ \frac{1}{4}(E_1 - E_2 - E_3 + E_4)\hat{\sigma}_z^1\hat{\sigma}_z^2 + \frac{1}{2}(V_{13} + V_{24})\hat{\sigma}_x^1 \\
&+ \frac{1}{2}(V_{12} + V_{24})\hat{\sigma}_x^2 + \frac{1}{2}(V_{12} - V_{34})\hat{\sigma}_z^1\hat{\sigma}_x^2 \\
&+ \frac{1}{2}(V_{13} - V_{24})\hat{\sigma}_x^1\hat{\sigma}_z^2 + \frac{1}{2}(V_{23} + V_{14})\hat{\sigma}_x^1\hat{\sigma}_x^2 + \frac{1}{2}(V_{23} - V_{14})\hat{\sigma}_y^1\hat{\sigma}_y^2,
\end{aligned}
\tag{5}
$$

where the superscripts of the Pauli matrices denote the qubit indices.

C. Variational Quantum Algorithm (VQA) for Quantum Dynamics

To simulate the exciton dynamics, we adopt the time-dependent VQA introduced in Ref. [32–34]. In this VQA, the time-dependent quantum state, $|\Psi(t)\rangle$, is approximated by a parametrized quantum state, $|\psi(\theta(t))\rangle$, i.e. $|\Psi(t)\rangle = \hat{T}e^{-i\int_0^t \hat{H}(t')dt'} |\Psi_0\rangle \approx \left|\psi(\vec{\theta}(t))\right\rangle$ where $\vec{\theta}(t) = [\theta_1(t), \theta_2(t), \theta_3(t)...]$ denotes the variational parameters at time t and $\hat{T}$ is the time-ordering operator. According to McLachlan's principle, the equation of motion for the variational parameters is obtained by minimizing the quantity $\|\left(i\frac{\partial}{\partial t} - \hat{H}(t)\right)|\psi(\theta)\|$ which results in

$$\vec{\theta}(t + \delta t) = \vec{\theta}(t) + \dot{\vec{\theta}}(t)\delta t; \ \dot{\vec{\theta}}(t) = \hat{M}^{-1}\vec{V}, \tag{6}$$

where the matrix elements of $\hat{M}$ and $\vec{V}$ are

$$\hat{M}_{kl} = \mathrm{Re}\left\langle \frac{\partial\psi(\vec{\theta})}{\partial\theta_k} \middle| \frac{\partial\psi(\vec{\theta})}{\partial\theta_l} \right\rangle ; \vec{V}_k = \mathrm{Im}\left\langle \psi(\vec{\theta}) \middle| \hat{H} \middle| \frac{\partial\psi(\vec{\theta})}{\partial\theta_k} \right\rangle . \tag{7}$$

The accuracy of VQA depends crucially on the choice of the wavefunction ansatz. Given the complexity of the encoded Hamiltonian, we need a powerful ansatz capable of accurately capturing the exciton dynamics, yet can be efficiently implemented in a quantum computer. Here we consider an ansatz of the form

$$|\psi(\theta)\rangle = \hat{U}(\vec{\theta})\,|\psi_0\rangle = \prod_k \hat{U}_k(\theta_k)\,|\psi_0\rangle = \prod_k \mathrm{e}^{i\theta_k\hat{R}_k}\,|\psi_0\rangle . \tag{8}$$

where $|\psi_0\rangle$ is the initial state of the wavefunction and $\hat{R}_k$ is some Pauli strings. In the numerical calculations in the following section, we consider all combinations of single and 2-qubit rotations, i.e. $\hat{R}_k \in \{\hat{\sigma}_a^m, \hat{\sigma}_a^m\hat{\sigma}_b^n\}$ for $a, b = x, y, z$ and all qubit combinations. Thus despite the fact the Hamiltonian could contain many-body interaction terms encompassing multiple qubits, only two-qubit rotations are required in the quantum state preparation.

We next show that the matrix elements of $\hat{M}$ and $\vec{V}$ can be efficiently measured in a quantum computer. We note that the derivative of each term in Eq. 8 is written as $\frac{\partial\hat{U}_k(\theta_k)}{\partial\theta_k} = i\hat{R}_k\hat{U}_k(\theta_k)$, therefore the matrix elements of $\hat{M}$ and $\vec{V}$ are (assuming $k < l$)

$$\begin{aligned}
\hat{M}_{kl} &= \mathrm{Re}\big(\,\langle\psi_0|\,\hat{U}_1^\dagger...\hat{U}_k^\dagger\hat{R}_k^\dagger...\hat{U}_L^\dagger\hat{U}_L..\hat{R}_l\hat{U}_l...\hat{U}_1\,|\psi_0\rangle\,\big) \\
&= \mathrm{Re}\big(\,\langle\psi_0|\,\hat{U}_1^\dagger...\hat{U}_k^\dagger\hat{R}_k^\dagger\hat{U}_{k+1}^\dagger...\hat{U}_l^\dagger\hat{R}_l\hat{U}_l...\hat{U}_1\,|\psi_0\rangle\,\big), \\
\vec{V}_k &= \mathrm{Im}\big(i\sum_j c_j\,\langle\psi_0|\,\hat{U}_1^\dagger...\hat{U}_L^\dagger\hat{h}_j\hat{U}_L..\hat{R}_k\hat{U}_k...\hat{U}_1\,|\psi_0\rangle\,\big),
\end{aligned} \tag{9}$$

where we have expressed the Hamiltonian as $\hat{H} = \sum_j c_j\hat{h}_j$. The quantities in Eq.9 are obtained in a quantum circuit via the Hadamard test, and the structures of the circuits are shown in Fig. 2.

D. Numerical Results

To demonstrate the capability of VQA in modelling exciton transport, we numerically simulate the exciton dynamics in a crystal of 64 T2 molecules, arranged in a $4 \times 4 \times 2$ super cell (each unit cell contains 2 molecules). The structure of the molecular crystal is
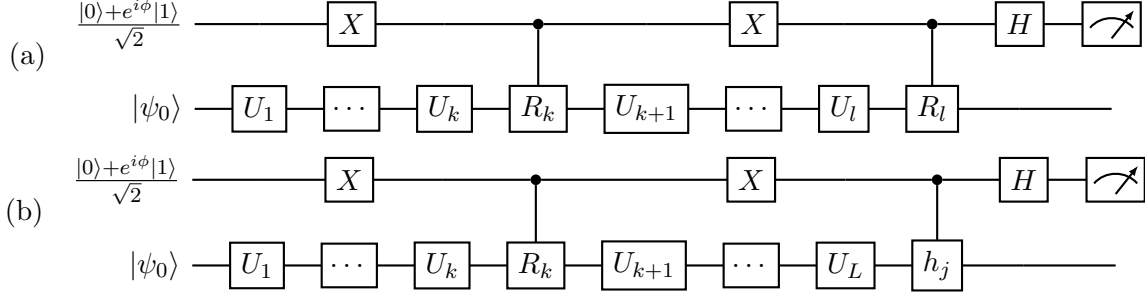
FIG. 2: Quantum circuits to compute the matrix elements of (a) $\hat{M}$ and (b) $\vec{V}$ in Eq. 9. The ancillary qubit is initialized in state $\frac{|0\rangle + e^{i\phi}|1\rangle}{\sqrt{2}}$. The phase factor ϕ is set to be 0 or $\pi/2$ in order to measure the real and imaginary components of the expectation values, respectively.

shown in the inset of Fig. 3a. The time-dependent exciton Hamiltonian is obtained via MD and TDDFT calculations, and the details of these calculations can be found in the Methods section. With the binary encoding scheme described in Section II B, the exciton Hamiltonian is encoded in 6 qubits, and a VQA simulation time-step of 0.04fs is used.

In our simulations, a molecule at the center of the molecular crystal is initially excited, and we study the time evolution of the exciton population in this molecule, the results are shown in Fig. 3a. The numerical result from VQA (red dashed line) is compared with the result obtained via exact diagonalization (solid black line). It is seen that the dynamics from VQA is in excellent agreement with that of exact calculation, confirming the capability of VQA in modelling exciton dynamics. From the population dynamics in Fig. 3a, we observe that the electronic excitation delocalizes rapidly into neighboring molecules, the entire process takes less than 100 fs. Despite the fast delocalization, clear oscillatory behavior due to quantum coherence is also seen within the first 40 fs.

We next investigate the inverse participation ratio (IPR) of the exciton wavefunction. IPR is a global quantity that measures the extent of wavefunction delocalization:

$$\text{IPR} = \frac{1}{\sum_m p_m^2}, \tag{10}$$

where p_m is the probability of locating the exciton in molecule m. If the exciton is evenly delocalized across N molecules, IPR $= N$ since $p_m = 1/N$. On the other hand, if an exciton is fully localized in one molecule then IPR $= 1$. Since p_m is equivalent to the probability of obtaining the corresponding qubit quantum state from the output of the quantum circuit (see Eq. 2), IPR is readily obtained from the distribution of the output states from a

quantum computer. In Fig. 3b, the IPR numerically computed with VQA is compared to exact diagonalization results, and we again observe good agreement, further demonstrating the ability of VQA in simulating the exciton dynamics. From Fig. 3b, it can be seen that IPR starts to plateau after around 40 fs due to the finite system size. Note that the maximum IPR in Fig. 3b is approximately 35, which is less than the number of molecules in the system because the disorder in inter-molecular couplings as well as dynamical fluctuations cause the exciton wavefunction unevenly distributed across all molecules, leading to a smaller IPR than the number of molecules.

We also study the dissipative exciton dynamics due to the interaction with phonon environment by averaging an ensemble of 100 pure state trajectories, the corresponding population and IPR dynamics are shown in Fig. 3c and d, respectively. We again observe nearly perfect agreement between the results from VQA and exact calculations, validating the capability of VQA in simulating exciton dynamics in complex environment. From Fig. 3c and d, it is seen that the oscillatory behaviors of the population and IPR dynamics have disappeared due to decoherence caused by exciton-phonon interactions. Decoherence is believed to be an important driving force for efficient energy transport in photosynthetic light-harvesting systems [44, 45].

E. Experimental Results on IBM Quantum Computers

We assess the capability of current digital quantum computers in simulating exciton dynamics by studying a linear chain of 4 T2 molecules with an IBM quantum computer. Due to the limitations of the actual quantum device, here, we consider a simplified model and assume a static system with identical nearest neighbor coupling of $V = 40$ meV and periodic boundary condition. This value of coupling corresponds to 2 T2 molecules separated by approximately 5.6Å and the plane of molecules are arranged in parallel to each other. Furthermore, we assume site energies of $E_1 = E_2$, $E_3 = E_4$ and $E_1 - E_3 = \Delta E = 20$meV. With these approximations, the 4-molecule system is encoded in 2 qubits and the resulting Hamiltonian is $H = \frac{\Delta E}{2}\sigma_z^1 + V\sigma_x^2 + V\sigma_x^1\sigma_x^2$. We use a wavefunction ansatz with only three variational parameters $\left|\psi(\vec{\theta})\right\rangle = e^{i\theta_3\sigma_x^1\sigma_x^2}e^{i\theta_2\sigma_x^2}e^{i\theta_1\sigma_z^1}\left|\psi_0\right\rangle$, corresponding to the popular Hamiltonian ansatz [50]. The compiled quantum circuits used in obtaining $\hat{M}$ and $\vec{V}$ in Eq. 7 can be found in Supplementary Materials (SM). Molecule 1 is initially excited, and
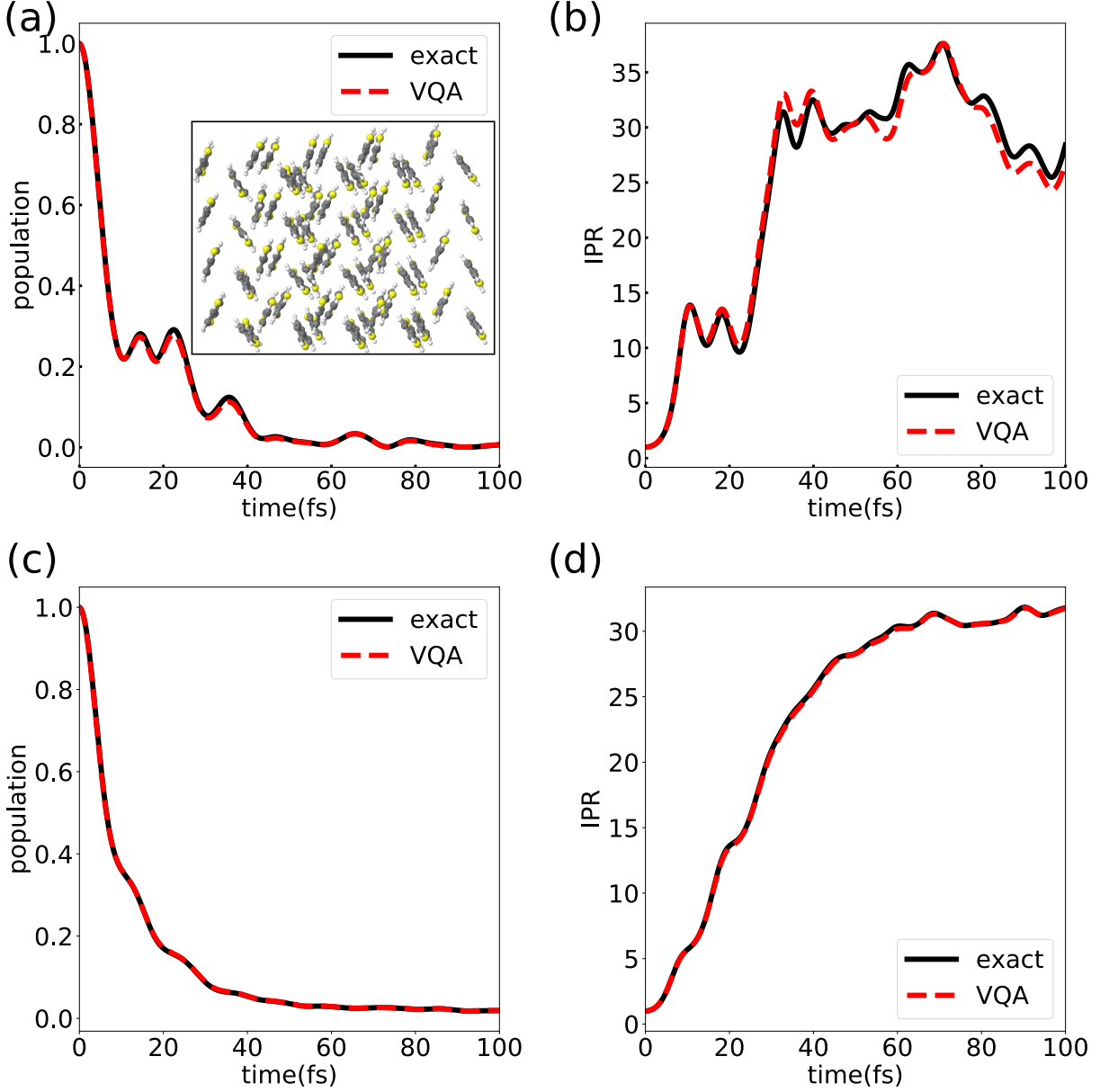
11

FIG. 3: Exciton dynamics in a molecular crystal of 64 bi-thiophene molecules obtained from exact calculations (black solid lines) and variational quantum algorithm (red dashed lines). (a) Exciton population dynamics in molecule where the exciton is initially located. (b) Time evolution of inverse participation ratio (IPR) defined in Eq. 10. (c) and (d) Dissipative exciton and IPR dynamics obtained by averaging over an ensemble of 100 pure state trajectories.

a time step of $\delta t = 1.97$fs is used (i.e. $3\hbar \text{eV}^{-1}$) throughout the simulations in this section. The quantum computer used here is the 5-qubit system code-named $ibmq\_rome$.

Fig. 4a displays the population dynamics computed by IBM quantum computer using
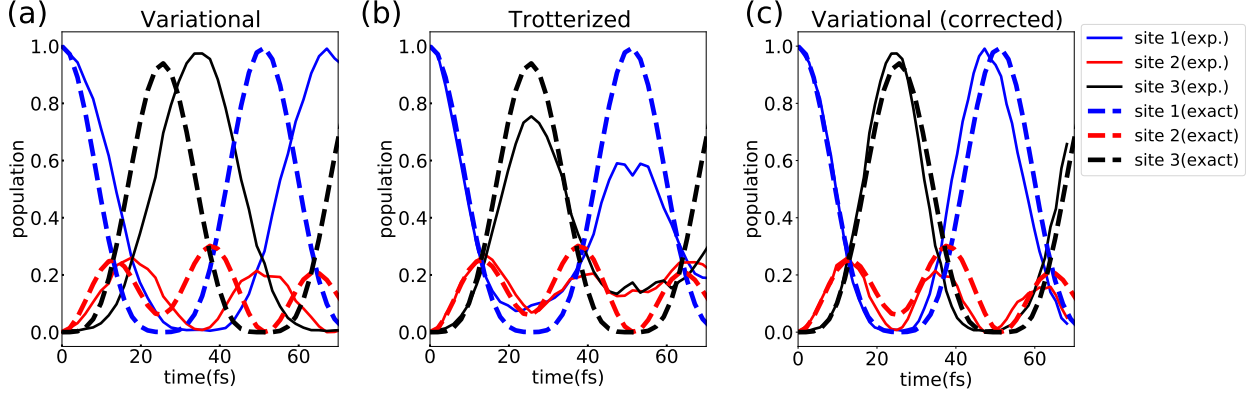
FIG. 4: Exciton population dynamics in a linear chain of 4 bi-thiophene molecules (encoded in 2 qubits) obtained from IBM quantum computer (solid lines) and from exact calculations (dashed lines). The experimental results are obtained using (a) variational quantum algorithm, (b) Trotter scheme and (c) variational quantum algorithm with error mitigation.

the VQA algorithm (solid lines). For comparison, we also include the exciton dynamics calculated with exact diagonalization (dashed lines). For clarity, we only show the populations dynamics of site 1 to site 3 since the population dynamics of site 4 is similar to that of site 2. The dynamics of site 4 population is found in SM. From Fig. 4a, it can be seen that though VQA correctly captures the amplitudes of the oscillations of different sites, the oscillation frequencies from VQA are smaller than that of the exact dynamics and this results in an overall right shift of the VQA dynamics. The accuracy of the VQA dynamics is principally determined by three factors: the expressive power of the wavefunction ansatz, error due to finite number of measurements and the imperfections of quantum devices. To identify the main source of error, we performed additional calculations (see SM) with noiseless quantum simulator and show that the discrepancy with exact results observed in Fig. 4a is largely due to the imperfection of the quantum devices. We observe that the noiseless simulator results using the same number of measurements are in good agreement with exact calculations.

It is also instructive to study the exciton dynamics with the standard Trotterization method by discretizing the evolution operator: $|\Psi(t)\rangle = \prod_n e^{-iH\delta t} |\Psi(0)\rangle$. For the 4-molecule system considered here, each discrete operator $e^{-iH\delta t} \approx e^{-iV\sigma_x^1\sigma_x^2\delta t}e^{-iV\sigma_x^1\delta t}e^{-i\Delta E\sigma_z^1\delta t}$ can then easily be implemented with single and two-qubit rotations. The Trotter results from IBM quantum computer are shown in Fig. 4b (dashed lines). As opposed to VQA, the results from the Trotterization scheme fail to capture the amplitudes of the oscillations, and the

decreasing amplitude indicates that decoherence effect is significant. On the other hand, from Fig. 4b, it is seen that the Trotterization approach captures the periods of the exciton dynamics since the peak and trough positions coincide with those from the numerically exact results.
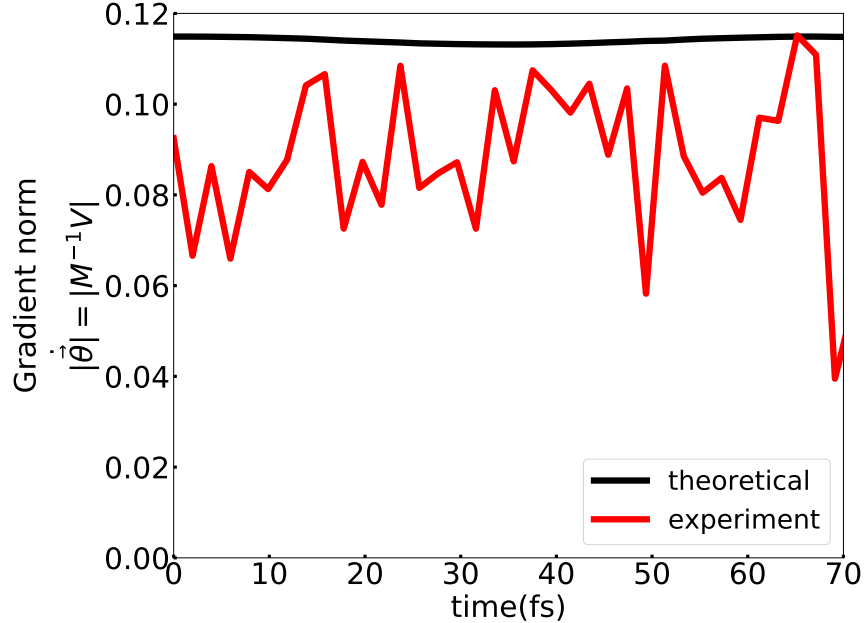

FIG. 5: The norms of gradient, $\dot{\vec{\theta}}$, obtained from IBM quantum computer (solid red line) and the theoretical values (solid black lines). The theoretical value is almost always larger than that of the experimental value due to errors in quantum hardware.

F.   Error Analysis and Mitigation

To identify the origin of the discrepancy between the VQA and exact dynamics in Fig. 4a, we investigate the norm of the gradient in Eq. 6, $\dot{\vec{\theta}} = \hat{M}^{-1}\vec{V}$, and the results are shown in Fig. 5. The red line denotes the magnitude of $|\dot{\vec{\theta}}|$ obtained from the IBM quantum computer whereas the black line is the theoretical value for the same set of variational parameters. It is found that the gradient norms from the quantum computer are almost always lower than the theoretical ones due to the errors in the quantum hardware.

To better understand the dependence of gradient, $\dot{\vec{\theta}} = \hat{M}^{-1}\vec{V}$, on noise level, λ, in quantum devices, we create an artificial noise model and perform noisy simulations using the IBM Qiskit quantum simulator [51]. The details of the noise model can be found in
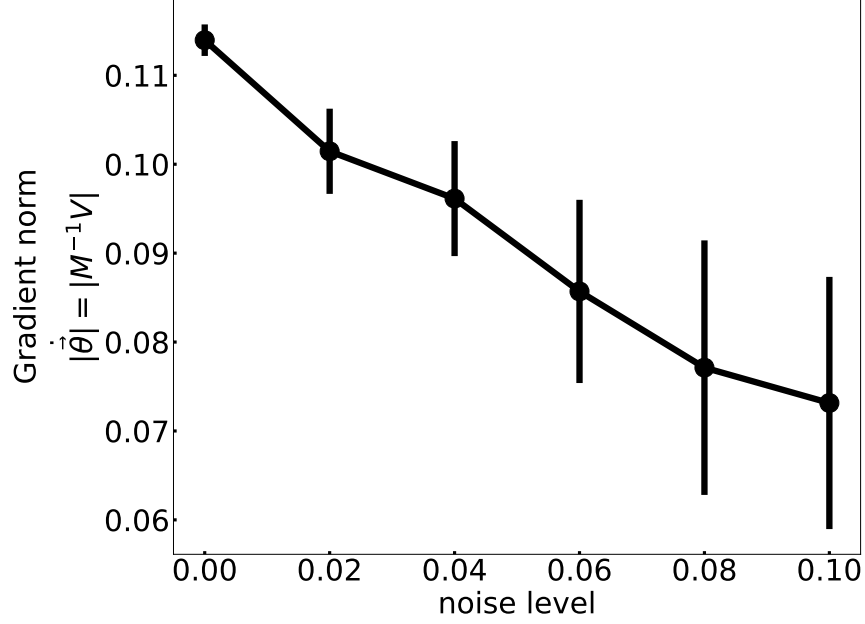
FIG. 6: Dependence of the gradient norm, $|\dot{\vec{\theta}}|$, as a function of noise level using an artificial noise model in quantum simulator. The error bars denotes the standard deviations from 100 independent simulations. The error bar at zero noise arises from the finite number of measurements.

SM. In Fig. 6, we compute the norm of gradient as a function of noise level, λ, using the variational parameters obtained experimentally at $t = 40\text{fs}$. We use 8192 shots in the simulations. It can be seen that the norm $|\dot{\vec{\theta}}|$ decreases monotonically as a function of λ, an observation consistent with the experimental observations that noise in quantum devices leads to an under-estimation of gradient norm. The under-estimation of the gradient seen in Fig. 5 therefore leads to an effective update time-step that is smaller than the actual time-step, i.e. $\delta t_{\text{eff}} < \delta t$, leading to the right-shift of the VQA dynamics compared to the exact results.

Next we show that this error can be partially mitigated by replacing δt with δt_{eff} in the equation of motion of the variational parameters, Eq. 6. Writing $\delta t_{\text{eff}} = \delta t / \alpha$ where the correction factor $\alpha > 1.0$, we propose extracting the optimal α from the short-time dynamics of the Trotter simulations. While the Trotter scheme is not suitable for NISQ devices due to the need for deep circuit depth, the short-time dynamics is expected to be more accurate than VQA since only small number of quantum gates are executed, and there is no need for the complicated Hadamard tests in constructing $\hat{M}$ and $\vec{V}$. Specifically, we choose the optimal α by minimizing the difference between site 1 populations obtained from VQA and

15

from the Trotter scheme, i.e.

$$\min_{\alpha} \int_0^{t_c} \left(p_1^{\text{VAQ}}(t) - p_1^{\text{Trotter}}(t) \right)^2 dt, \tag{11}$$

where we use a cut-off time of $t_c = 20\text{fs}$. In our case, we found the optimal α to be 1.42, a value close to the ratio between the time-averaged theoretical and experimental norms shown in Fig. 5 (i.e. 1.34). The corrected VQA dynamics are shown in Fig. 4c, it can be seen that the corrected results accurately reproduce the population evolution of all the sites in the system though only site 1 population is used to extract the optimal α. Thus by combining the results from both algorithms, the error-mitigated exciton dynamics can be significantly more accurate than the results from either VQA or Trotter scheme.

In SM, we demonstrate the above the error mitigation method in different system by simulating the dynamics of transverse field Ising (TFI) model with noisy simulator. We again obtained a much improved results compared to the simulations without error mitigation, suggesting the generality of our approach. The error mitigation technique above can be generalized to more complex systems in which the correction factor, α, may not be a simple constant but could vary with time. In such cases, we could divide the total simulation time into multiple simulation windows. For each simulation window, we perform a separate Trotter simulation to extract the optimal shift factor for that particular segment, with initial condition being the variational quantum state at the beginning of the time window.

III. DISCUSSIONS AND CONCLUSIONS

Most of the recent experimental and theoretical NISQ research for chemical applications focus on finding the ground or low energy states of molecular systems. Here we expand the scope of applications for near-term digital quantum computers to time-dependent processes in many-body chemical systems. Compared to the ground state calculations, simulating quantum dynamics is typically a more challenging task as it often involves the participation of all quantum states. NISQ algorithms for ground state simulation like the popular variational quantum eigensolver (VQE) involve minimizing the expectation value of the Hamiltonian for a given variational wavefunction, and the optimization path is usually not important as long as the final optimized wavefunction is a good approximation of the true ground state wavefunction of the Hamiltonian. On the other hand, VQA for quantum dy-

namics requires the path of the variational wavefunction to closely match that of the exact dynamics throughout the entire evolution, and a small discrepancy can easily lead to a very different quantum state at a later time.

Studying energy transfer in molecular systems is a fitting example to test the capability of quantum computers in simulating quantum dynamics in chemical systems. Understanding energy transfer process in molecular systems is important with a wide range of practical applications, e.g. design of efficient OPVs and OLEDs. However, accurate simulation of exciton dynamics for realistic systems is challenging in classical computers. The presence of disorder and long-range couplings in molecular systems renders Bloch's band theory commonly used in condensed matter physics inapplicable due to the lack of symmetry. Coarse-grained or classical models can provide important physical insights, but fail to capture the quantum mechanical properties and chemical details of the actual materials. Quantum computers could therefore potentially overcome these computational challenges. With the binary encoding scheme, an exciton Hamiltonian of N sites can be encoded in $\log_2(N)$ qubits. In other words, three dimensional molecular systems consisting of millions of sub-units can be encoded in as few as tens of qubits. This opens the possibility of studying exciton transport in systems of experimentally relevant sizes fully quantum mechanically.

While our numerical calculations affirms the capability of the VQA in simulating quantum dynamics of molecular systems, running the algorithm on actual quantum computer provides us with important insights into the robustness of the algorithm against device imperfections. While experimental demonstration of hybrid algorithms for ground-state quantum chemistry has been performed on systems that exceed 10 qubits [13], digital quantum simulations of time-dependent chemistry problems has been lacking. In fact, the time-dependent VQA has only been recently demonstrated on a 2-qubit Ising model in the adiabatic limit [34]. Indeed our experimental results with IBM quantum devices demonstrate that, despite only short circuit depth is needed in VQA, the error rates in current quantum computers are still too large to accurately simulate the quantum dynamics of molecular Hamiltonians with a few qubits.

Despite the failure of VQA (without error mitigation) in capturing the correct quantum dynamics, analysis of the results provides important insights into the source of errors and how to mitigate them. Our investigation reveals that the deviation from the exact result arises from the under-estimation of the gradients, $\dot{\vec{\theta}}$ as shown in Fig. 5. We further show that

this error in gradient estimation can be largely remedied by extracting a correction factor from the short-time dynamics of the Trotter simulation. To the best of our knowledge, our work constitutes the first demonstration that energy transport in realistic chemical systems can be accurately simulated in a digital quantum computer.

Recently there have been several experimental demonstration of error mitigation techniques for ground-state quantum chemistry problems with encouraging results [10, 13], our work provides an additional tool to combat quantum device errors for dynamical simulations in chemistry. The effectiveness of the error mitigation method shown in Fig. 4c also opens the door to the possibility of improving the accuracy of quantum simulations by combining the experimental results from different quantum algorithms. Unlike many other error mitigation methods that require multiple executions of the quantum circuits to construct the statistical profile of the errors, our error mitigation method only requires running each quantum algorithm once. Thus this is particularly appealing for cloud based NISQ devices in which the queue time and cost could be significant. This error mitigation method can be extended to simulate other time-dependent phenomena in biology and chemistry such as spectroscopy, chemical reaction and charge transfer. A systematic approach to perform this error mitigation technique in combination with other error mitigation methods will be a fruitful future endeavor, though it is beyond the scope of this current work.

To conclude, in this work, we propose the simulation of energy transfer dynamics in molecular systems with digital quantum computers. We first perform multi-scale calculations to obtain the exciton Hamiltonian of an N-molecule. The Hamiltonian is then mapped onto $\log_2(N)$ qubits with a binary encoding scheme, and we use a hybrid time-dependent VQA to simulate the time evolution of the encoded Hamiltonian. Our numerical example affirms the feasibility of this approach. Despite the short circuit depth in VQA, our experimental results with IBM quantum computer show that current quantum devices are still plagued with too much noise for a good simulation of the dynamics of these quantum many-body systems. We propose a new error mitigation technique for correcting the VQA dynamics with the information extracted from the short-time dynamics of Trotter simulation. We demonstrate that the corrected VQA dynamics is significantly improved and capable of capturing the true dynamics of the excitonic system. Our work extends the scope of applications of NISQ devices to time-dependent processes in chemical systems, and opens the door to new error mitigation technique that combines the experimental results of multiple quantum algorithms.

IV. METHODS

To construct the time-dependent Frenkel exciton Hamiltonian, classical MD simulation was performed for a T2 crystal with 64 T2 molecules in the simulation box. The initial simulation box was set up as a $4 \times 4 \times 2$ super cell based on the experimental [52] crystal structure of T2 (CSD identifier: DTENYL02). OPLS/2005 force field was employed in the simulation as it can reasonably reproduce the torsional potential energy surface of T2 predicted from the localized second order Møller-Plesset perturbation theory (LMP2) [53]. The MD simulation was performed with the Desmond package 3.6 [54] in the NVT ensemble at 133 K, the crystal temperature in the experiment [52]. Temperature was maintained by the Nosé-Hoover thermostat with a coupling constant of 2.0 ps. Periodic boundary condition was applied to the monoclinic simulation box, and the particle-mesh Ewald (PME) method was employed for electrostatic interactions. The simulation time step was 1 fs, and the configurations were saved every 2 fs during the 10-ps production run. A snapshot of the MD configuration is given in Fig. 3a.

The site energy in the Frenkel exciton Hamiltonian is approximated by the lowest-lying excited-state energy of each T2 in the system, which was computed by TDDFT with the Tamm-Dancoff approximation (TDA) using CAM-B3LYP/6-31+G(d). In our previous work [55] we have shown that the excited-state energy of T2 predicted by CAM-B3LYP/6-31+G(d) agrees well with that from a correlated wavefunction method (CC2 method). All the quantum chemical calculations were performed with the PySCF program [56], and density fitting was used with the heavy-aug-cc-pvdz-jkfit auxiliary basis set implemented in PySCF. In estimating the excitonic coupling between the local excitations on two T2 molecules (m and n), V_{mn}, we computed the Coulomb coupling via[57]

$$V_{mn} \approx 2 \sum_{iajb} X_{ia}^{(m)} X_{jb}^{(n)} \iint \psi_i^{(m)}(\vec{r}_1)\psi_a^{(m)}(\vec{r}_1)\frac{1}{|\vec{r}_1 - \vec{r}_2|}\psi_j^{(n)}(\vec{r}_2)\psi_b^{(n)}(\vec{r}_2)d\vec{r}_1 d\vec{r}_2, \qquad (12)$$

where $X_{ia}^{(m)}$ is the excitation amplitude for the electronic transition from the occupied molecular orbital (MO), $\psi_i^{(m)}$, to the virtual MO, $\psi_a^{(m)}$, of molecule m. In using the Coulomb coupling to approximate the excitonic coupling, we have neglected the contributions from the Hartree-Fock exchange and the exchange-correlation of the employed functional, CAM-B3LYP. The computations of site energies and couplings were performed for the 5,000 frames harvested from the MD simulation, leading to a trajectory of time-dependent Frenkel ex-

citon Hamiltonian. It is worth noting that even though the computational cost of constructing the exciton Hamiltonian through quantum chemistry calculations scales linearly with the number of sub-units (assuming that the inter-molecular couplings are negligible beyond certain distance), the computational cost itself is still high for large systems. However, several statistical and machine-learning methods have been developed to overcome this difficulty [55, 57, 58]. Once sufficient quantum chemistry data have been generated, the remaining matrix elements in the exciton Hamiltonians can be obtained through these statistical or machine learning methods with very high accuracy.

V. ACKNOWLEDGMENT

[1] Lanyon, B. P. *et al.* Towards quantum chemistry on a quantum computer. *Nature Chemistry* **2**, 106–111 (2010).

[2] Aspuru-Guzik, A. Simulated Quantum Computation of Molecular Energies. *Science* **309**, 1704–1707 (2005).

[3] Kassal, I., Whitfield, J. D., Perdomo-Ortiz, A., Yung, M. H. & Aspuru-Guzik, A. Simulating chemistry using quantum computers. *Annual Review of Physical Chemistry* **62**, 185–207 (2011).

[4] McArdle, S., Endo, S., Aspuru-Guzik, A., Benjamin, S. C. & Yuan, X. Quantum computational chemistry. *Reviews of Modern Physics* **92**, 15003 (2020).

[5] Cao, Y. *et al.* Quantum Chemistry in the Age of Quantum Computing. *Chemical Reviews* **119**, 10856–10915 (2019).

[6] Bauer, B., Bravyi, S., Motta, M. & Kin-Lic Chan, G. Quantum Algorithms for Quantum Chemistry and Quantum Materials Science. *Chemical Reviews* **120**, 12685–12717 (2020).

[7] Cerezo, M. *et al.* Variational Quantum Algorithms 1–29 (2020). arXiv:2012.09265.

[8] Peruzzo, A. *et al.* A variational eigenvalue solver on a photonic quantum processor. *Nature Communications* **5** (2014).

[9] Kandala, A. *et al.* Hardware-efficient variational quantum eigensolver for small molecules and quantum magnets. *Nature* **549**, 242–246 (2017).

[10] Kandala, A. *et al.* Error mitigation extends the computational reach of a noisy quantum processor. *Nature* **567**, 491–495 (2019).

[11] O'Malley, P. J. *et al.* Scalable quantum simulation of molecular energies. *Physical Review X* **6**, 1–13 (2016).

[12] Motta, M. *et al.* Determining eigenstates and thermal states on a quantum computer using quantum imaginary time evolution. *Nature Physics* **16**, 205–210 (2020). arXiv:1901.07653.

[13] AI Quantum, G. Hartree-Fock on a superconducting qubit quantum computer. *Science* **369**, 1084–1089 (2020).

[14] Hempel, C. *et al.* Quantum chemistry calculations on a trapped-ion quantum simulator. *Phys. Rev. X* **8**, 31022 (2018).

[15] Parrish, R. M., Hohenstein, E. G., McMahon, P. L. & Martínez, T. J. Quantum Computation

of Electronic Transitions Using a Variational Quantum Eigensolver. *Physical Review Letters* **122**, 230401 (2019).

[16] Takeshita, T. *et al.* Increasing the Representation Accuracy of Quantum Simulations of Chemistry without Extra Quantum Resources. *Phys. Rev. X* **10**, 11004 (2020).

[17] O'Brien, T. E. *et al.* Calculating energy derivatives for quantum chemistry on a quantum computer. *npj Quantum Information* **5** (2019).

[18] Grimsley, H. R., Economou, S. E., Barnes, E. & Mayhall, N. J. An adaptive variational algorithm for exact molecular simulations on a quantum computer. *Nature Communications* **10** (2019).

[19] Nam, Y. *et al.* Ground-state energy estimation of the water molecule on a trapped-ion quantum computer. *npj Quantum Information* **6**, 1–6 (2020).

[20] McCaskey, A. J. *et al.* Quantum chemistry as a benchmark for near-term quantum computers. *npj Quantum Information* **5**, 99 (2019).

[21] Hsieh, C. Y., Sun, Q., Zhang, S. & Lee, C. K. Unitary-coupled restricted Boltzmann machine ansatz for quantum simulations. *npj Quantum Information* (2021).

[22] Mukamel, S. *Principles of Nonlinear Optical Spectroscopy* (Oxford, New York, 1995).

[23] Nitzan, A. *Chemical Dynamics in Condensed Phases: Relaxation, Transfer, and Reactions in Condensed Molecular Systems.* Oxford Graduate Texts (OUP Oxford, 2013).

[24] Gatti, F., Lasorne, B., Meyer, H.-D. & Nauts, A. *Applications of Quantum Dynamics in Chemistry*, vol. 98 of *Lecture Notes in Chemistry* (Springer International Publishing, Cham, 2017). URL `http://link.springer.com/10.1007/978-3-319-53923-2`.

[25] Heya, K., Nakanishi, K. M., Mitarai, K. & Fujii, K. Subspace Variational Quantum Simulator (2019). arXiv:1904.08566.

[26] Zhang, Z.-J., Sun, J., Yuan, X. & Yung, M.-H. Low-depth Hamiltonian Simulation by Adaptive Product Formula (2020). arXiv:2011.05283.

[27] Ollitrault, P. J., Mazzola, G. & Tavernelli, I. Nonadiabatic Molecular Quantum Dynamics with Quantum Computers. *Physical Review Letters* **125**, 260511 (2020).

[28] Lloyd, S. Universal Quantum Simulators. *Science* **273**, 1073–1078 (1996).

[29] Childs, A. M. & Wiebe, N. Hamiltonian Simulation Using Linear Combinations of Unitary Operations. *Quantum Info. Comput.* **12**, 901–924 (2012).

[30] Low, G. H. & Chuang, I. L. Optimal Hamiltonian Simulation by Quantum Signal Processing.

Physical Review Letters **118**, 010501 (2017).

[31] Low, G. H. & Chuang, I. L. Hamiltonian Simulation by Qubitization. *Quantum* **3**, 163 (2019).

[32] Li, Y. & Benjamin, S. C. Efficient Variational Quantum Simulator Incorporating Active Error Minimization. *Physical Review X* **7**, 021050 (2017).

[33] Endo, S., Sun, J., Li, Y., Benjamin, S. C. & Yuan, X. Variational Quantum Simulation of General Processes. *Physical Review Letters* **125**, 010501 (2020). arXiv:1812.08778.

[34] Chen, M.-c. *et al.* Demonstration of Adiabatic Variational Quantum Computing with a Superconducting Quantum Coprocessor. *Physical Review Letters* **125**, 180501 (2020).

[35] Temme, K., Bravyi, S. & Gambetta, J. M. Error Mitigation for Short-Depth Quantum Circuits. *Physical Review Letters* **119**, 180509 (2017).

[36] McClean, J. R., Kimchi-Schwartz, M. E., Carter, J. & de Jong, W. A. Hybrid quantum-classical hierarchy for mitigation of decoherence and determination of excited states. *Physical Review A* **95**, 042308 (2017).

[37] Kim, C., Park, K. D. & Rhee, J.-K. Quantum Error Mitigation With Artificial Neural Network. *IEEE Access* **8**, 188853–188860 (2020).

[38] Ostroverkhova, O. Organic Optoelectronic Materials: Mechanisms and Applications. *Chemical Reviews* **116**, 13279–13412 (2016).

[39] Mikhnenko, O. V., Blom, P. W. & Nguyen, T. Q. Exciton diffusion in organic semiconductors. *Energy and Environmental Science* **8**, 1867–1888 (2015).

[40] Deotare, P. B. *et al.* Nanoscale transport of charge-transfer states in organic donor-acceptor blends. *Nature Materials* **14**, 1130–1134 (2015).

[41] Perepichka, I. F., Perepichka, D. F. & Meng, H. *Thiophene-Based Materials for Electroluminescent Applications*, vol. 2 (John Wiley & Sons, Ltd, Chichester, UK, 2009). URL `http://doi.wiley.com/10.1002/9780470745533.ch19`.

[42] Shi, L. & Willard, A. P. Modeling the effects of molecular disorder on the properties of Frenkel excitons in organic molecular semiconductors. *The Journal of Chemical Physics* **149**, 094110 (2018).

[43] Sisto, A., Glowacki, D. R. & Martinez, T. J. Ab initio nonadiabatic dynamics of multi-chromophore complexes: A scalable graphical-processing-unit-accelerated exciton framework. *Accounts of Chemical Research* **47**, 2857–2866 (2014).

[44] Mohseni, M., Rebentrost, P., Lloyd, S. & Aspuru-Guzik, A. Environment-assisted quantum

walks in photosynthetic energy transfer. *Journal of Chemical Physics* **129** (2008).

[45] Rebentrost, P., Mohseni, M., Kassal, I., Lloyd, S. & Aspuru-Guzik, A. Environment-assisted quantum transport. *New Journal of Physics* **11** (2009).

[46] Chin, A. W. *et al.* The role of non-equilibrium vibrational structures in electronic coherence and recoherence in pigment-protein complexes. *Nature Physics* **9**, 113–118 (2013).

[47] McArdle, S., Mayorov, A., Shan, X., Benjamin, S. & Yuan, X. Digital quantum simulation of molecular vibrations. *Chemical Science* **10**, 5725–5735 (2019). arXiv:1811.04069.

[48] Sawaya, N. P. & Huh, J. Quantum Algorithm for Calculating Molecular Vibronic Spectra. *Journal of Physical Chemistry Letters* **10**, 3586–3591 (2019).

[49] Sawaya, N. P. *et al.* Resource-efficient digital quantum simulation of d-level systems for photonic, vibrational, and spin-s Hamiltonians. *npj Quantum Information* **6**, 1–13 (2020).

[50] Wecker, D., Hastings, M. B. & Troyer, M. Progress towards practical quantum variational algorithms. *Physical Review A* **92**, 042303 (2015).

[51] Abraham, H. *et al.* Qiskit: An Open-source Framework for Quantum Computing (2019).

[52] Pelletier, M. & Brisse, F. Bithiophene at 133 K. *Acta Crystallographica Section C Crystal Structure Communications* **50**, 1942–1945 (1994).

[53] DuBay, K. H. *et al.* Accurate Force Field Development for Modeling Conjugated Polymers. *Journal of Chemical Theory and Computation* **8**, 4556–4569 (2012).

[54] Bowers, K. J. *et al.* Scalable algorithms for molecular dynamics simulations on commodity clusters. In *Proceedings of the 2006 ACM/IEEE conference on Supercomputing - SC '06*, 84 (ACM Press, New York, New York, USA, 2006).

[55] Lu, C. *et al.* Deep Learning for Optoelectronic Properties of Organic Semiconductors. *Journal of Physical Chemistry C* **124**, 7048–7060 (2020).

[56] Sun, Q. *et al.* PySCF: the Python-based simulations of chemistry framework. *Wiley Interdisciplinary Reviews: Computational Molecular Science* **8**, e1340 (2018).

[57] Farahvash, A., Lee, C. K., Sun, Q., Shi, L. & Willard, A. P. Machine learning Frenkel Hamiltonian parameters to accelerate simulations of exciton dynamics. *Journal of Chemical Physics* **153** (2020).

[58] Lee, C. K. & Willard, A. P. Representing the Molecular Signatures of Disordered Molecular Semiconductors in Size-Extendable Models of Exciton Dynamics. *The Journal of Physical Chemistry B* **124**, 5238–5245 (2020).

Supplementary Materials: Quantum Simulations of Energy Transfer in Molecular Systems with Digital Quantum Computers

Chee-Kong Lee[*]

Tencent America, Palo Alto, CA 94306, United States

Jonathan Wei Zhong Lau[†]

Centre for Quantum Technologies, National University of Singapore, 117543, Singapore

Liang Shi[‡]

Chemistry and Chemical Biology, University of California,

Merced, California 95343, United States

Leong Chuan Kwek[§]

Centre for Quantum Technologies, National University of Singapore, 117543, Singapore

National Institute of Education, Nanyang Technological University,

1 Nanyang Walk, Singapore 637616 and

MajuLab, CNRS-UNS-NUS-NTU International Joint Research Unit, UMI 3654, Singapore

[*]Electronic address: cheekonglee@tencent.com

[†]Electronic address: e0032323@u.nus.edu

[‡]Electronic address: lshi4@ucmerced.edu

[§]Electronic address: cqtklc@nus.edu.sg

I. ARTIFICIAL NOISE MODEL

In Fig. 6 of the main text we investigate the dependence of gradient, $\dot{\vec{\theta}} = \hat{M}^{-1}\vec{V}$, on noise level using an artificial noise model with IBM Qiskit quantum simulator [1]. The artificial noise model was created using the tools in Qiskit Aer noise model. Specifically in the noise model, we defined an overall noise parameter λ, where $0 \leq \gamma \leq 1$. This parameter controls the depolarizing error that is added to all single and two qubit rotations and control gates (e.g. CNOT gate). The map for the depolarizing channel is

$$E_{\text{depolarizing}}(\rho) = (1 - \lambda)\rho + \lambda \text{Tr}[\rho]I. \tag{1}$$

The depolarizing error, λ, is therefore the probability that a single qubit, after undergoing a rotation, will be replaced by the completely mixed state. It is usually considered to be the quantum version of the independent bit flip error in classical devices.

II. ADDITIONAL RESULTS FROM IBM QUANTUM COMPUTER

The dynamics of site 4 population in Sec. II E obtained from variational quantum algorithm (VQA), Trotter scheme and corrected VQA are shown in Fig. 1.
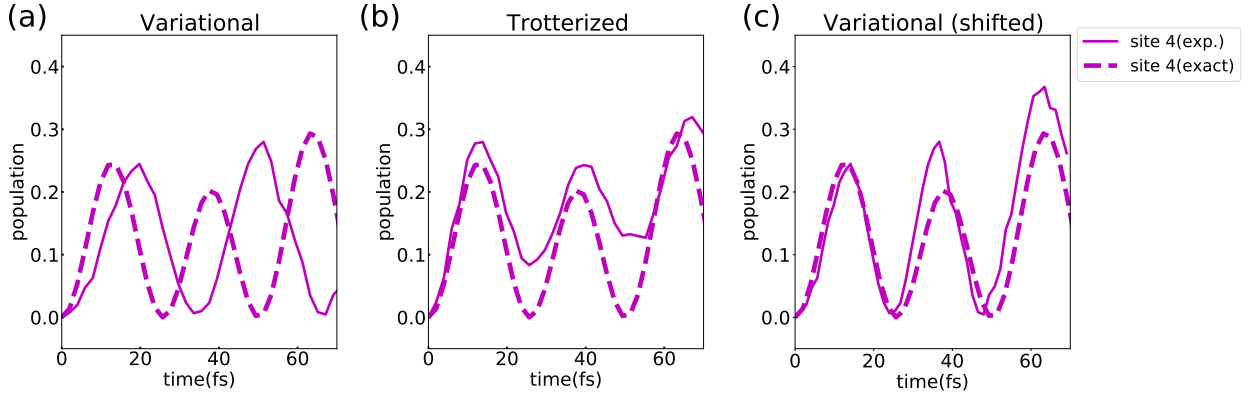
FIG. 1: The dynamics of site 4 population in Sec. II E obtained from (a) variational quantum algorithm (VQA), (b) Trotter scheme and (c) corrected VQA.

III. QUANTUM CIRCUITS FOR THE 4-MOLECULE SYSTEMS

For the 2-qubit simulations in Sec. II E in the main text, the compiled quantum circuits for computing the matrix elements of $\hat{M}$ are shown in Fig. 2, 3 and 4.
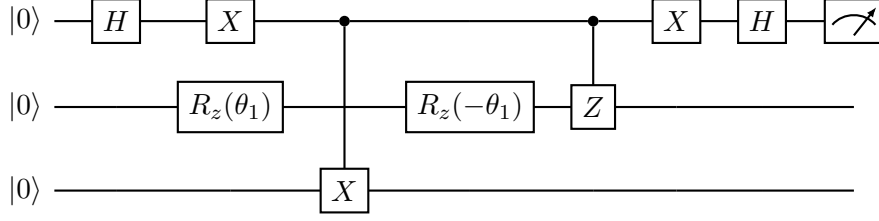
FIG. 2: Quantum circuit for computing $\text{Re}(\langle \frac{\partial \psi}{\partial \theta_1} | \frac{\partial \psi}{\partial \theta_2} \rangle)$.
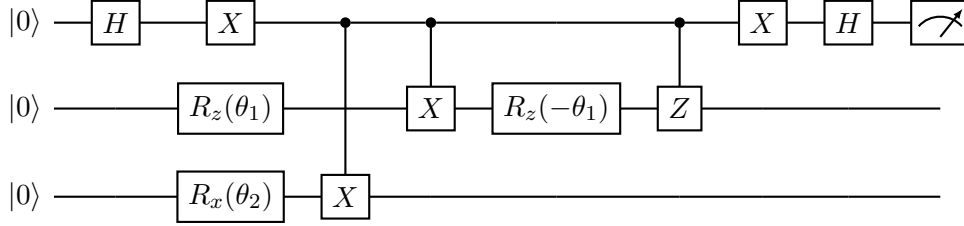

FIG. 3: Quantum circuit for computing $\text{Re}(\langle \frac{\partial \psi}{\partial \theta_1} | \frac{\partial \psi}{\partial \theta_3} \rangle)$.
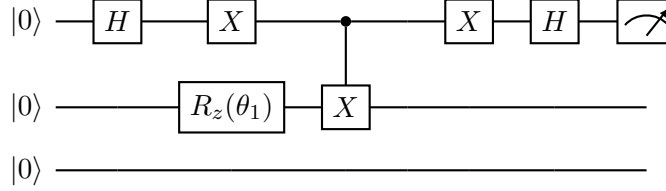

FIG. 4: Quantum circuit for computing $\text{Re}(\langle \frac{\partial \psi}{\partial \theta_2} | \frac{\partial \psi}{\partial \theta_3} \rangle)$.

where X, Y and Z denote the Pauli matrices.

Nine quantum circuits are needed for computing $\vec{V}$ vector elements since the Hamiltonian is a linear combination of 3 Pauli terms, so the measurement of each vector element requires 3 different quantum circuits. For example, the quantum circuits for measuring $\langle \frac{\partial \psi}{\partial \theta_1} | H | \psi \rangle = \frac{\Delta E}{2} \langle \frac{\partial \psi}{\partial \theta_1} | Z_1 | \psi \rangle + V \langle \frac{\partial \psi}{\partial \theta_1} | X_1 X_2 | \psi \rangle + V \langle \frac{\partial \psi}{\partial \theta_1} | X_2 | \psi \rangle$ are displayed in Fig. 5, 6 and 7.
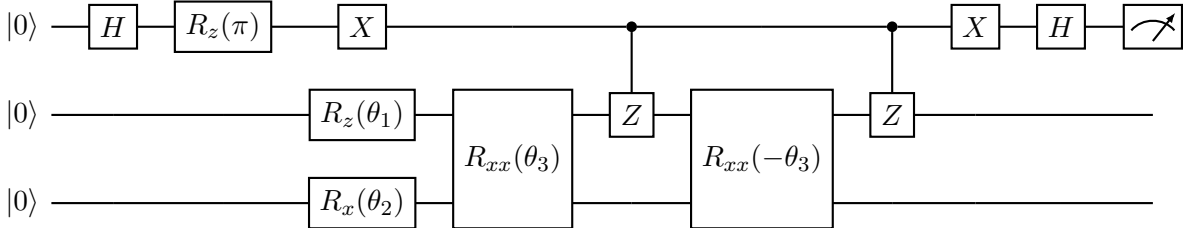

FIG. 5: Quantum circuit for computing $\text{Im}(\langle \frac{\partial \psi}{\partial \theta_1} | Z_1 | \psi \rangle)$.
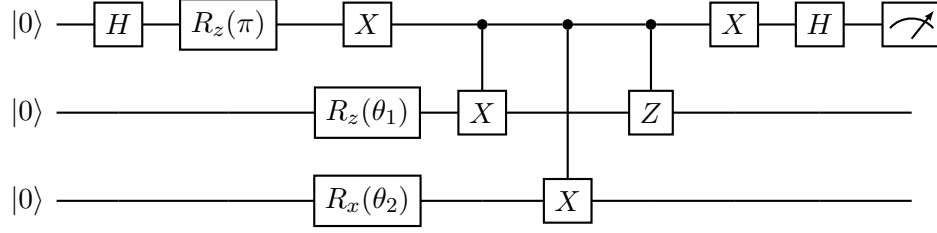
FIG. 6: Quantum circuit for computing $\text{Im}(\langle\frac{\partial\psi}{\partial\theta_1}|\,X_1 X_2\,|\psi\rangle)$.
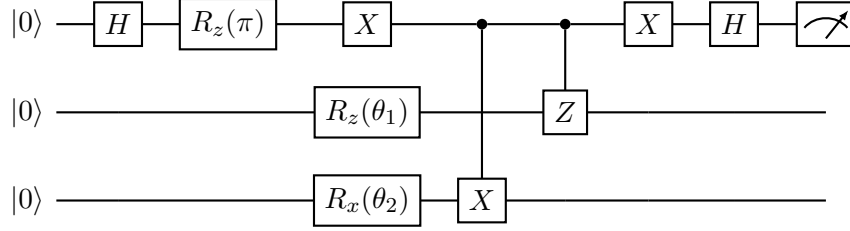

FIG. 7: Quantum circuit for computing $\text{Im}(\langle\frac{\partial\psi}{\partial\theta_1}|\,X_2\,|\psi\rangle)$.

IV. MITIGATION OF MEASUREMENT ERRORS

Before we performed any quantum simulations with the IBM quantum computers, we calibrated the measurement noise with a calibration matrix W on a daily basis. We first express the probabilities of obtaining the basis states $|00\rangle$, $|01\rangle$, $|10\rangle$ and $|11\rangle$ from a quantum circuit in a vector C_{noisy}. Next we find the matrix W that relates the probability vector C_{noisy} with the ideal measurement outcome without errors C_{ideal}, i.e. $C_{noisy} = WC_{ideal}$. To obtain the matrix W for the 2-qubit case, we independently prepare each of the input states $|00\rangle$, $|01\rangle$, $|10\rangle$ and $|11\rangle$, and measure that probability for each outcome.

V. SIMULATION RESULTS WITH NOISELESS SIMULATOR

We repeat the VQA simulation of the 4-site system using the noiseless simulator in IBM Qiskit quantum simulator, and the results are shown in Fig. 8. The number of shots used is 8192. It can be seen that the noiseless simulator results are in good agreement with the exact calculations, indicating the error observed in Fig. 4a in the main text does not come from the choice of wavefunction ansatz or the finite number of shots.
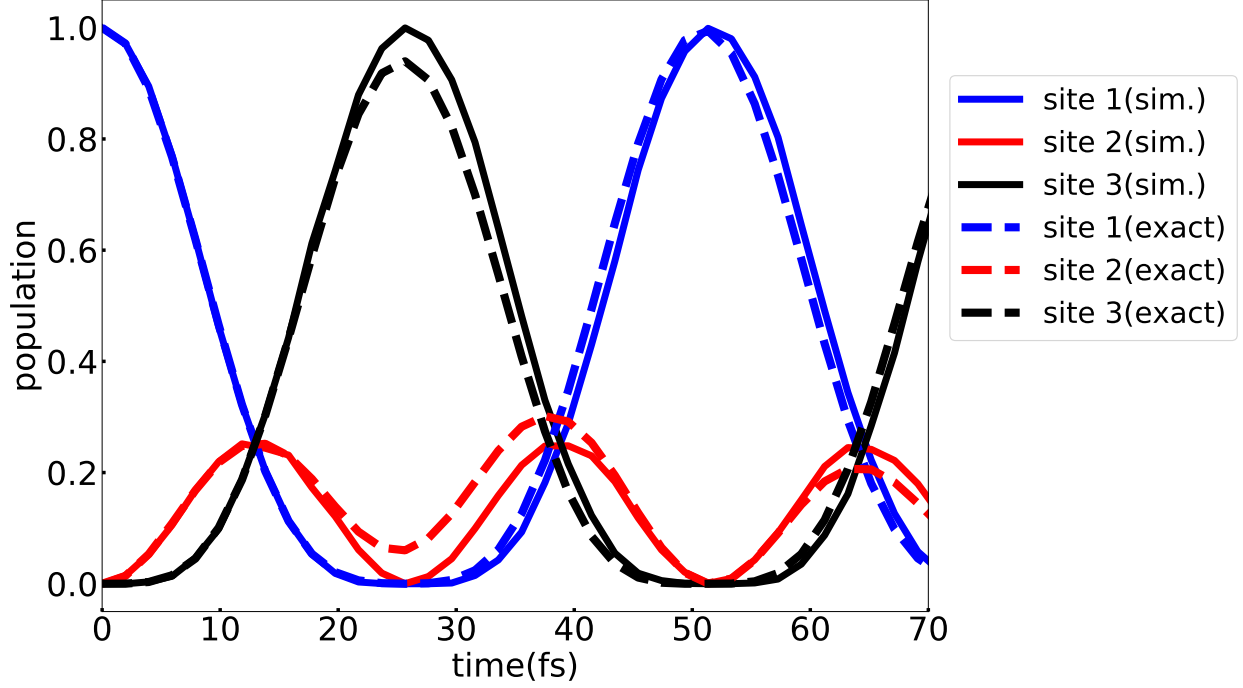
4

FIG. 8: Population dynamics of the 4-site model obtained from VQA using the IBM Qiskit noiseless simulator (dashed lines). The solid lines are results from numerically exact calculations.

VI.   SIMULATION OF TRANSVERSE FIELD ISING MODEL

In this section we simulate the dynamics of a 2-spin transverse field Ising (TFI) model with noisy simulator described in Sec. I to demonstrate the generality of the proposed error mitigation method. The Hamiltonian of the TFI model is given by $H = h(\sigma_x^1 + \sigma_x^2) + J\sigma_z^1\sigma_z^2$ where h is the magnitude of the transverse magnetic field and J is the interaction strength. Here we use $h = 0.5$, $J = 0.5$, a noise level of $\lambda = 0.01$, a Hamiltonian ansatz with depth 2 and time-step of 0.1. The system is initialized in state $|00\rangle$ and we investigate the probability of obtaining state $|00\rangle$ at time t, the results are shown in Fig. 9. It can be seen that quantum dynamics obtained from the VQA with error mitigation (red) is more accurate than the results from the VQA without error mitigation (blue) and the Trotter algorithm (green). This suggests our error mitigation approach can be used for general quantum dynamical simulations.
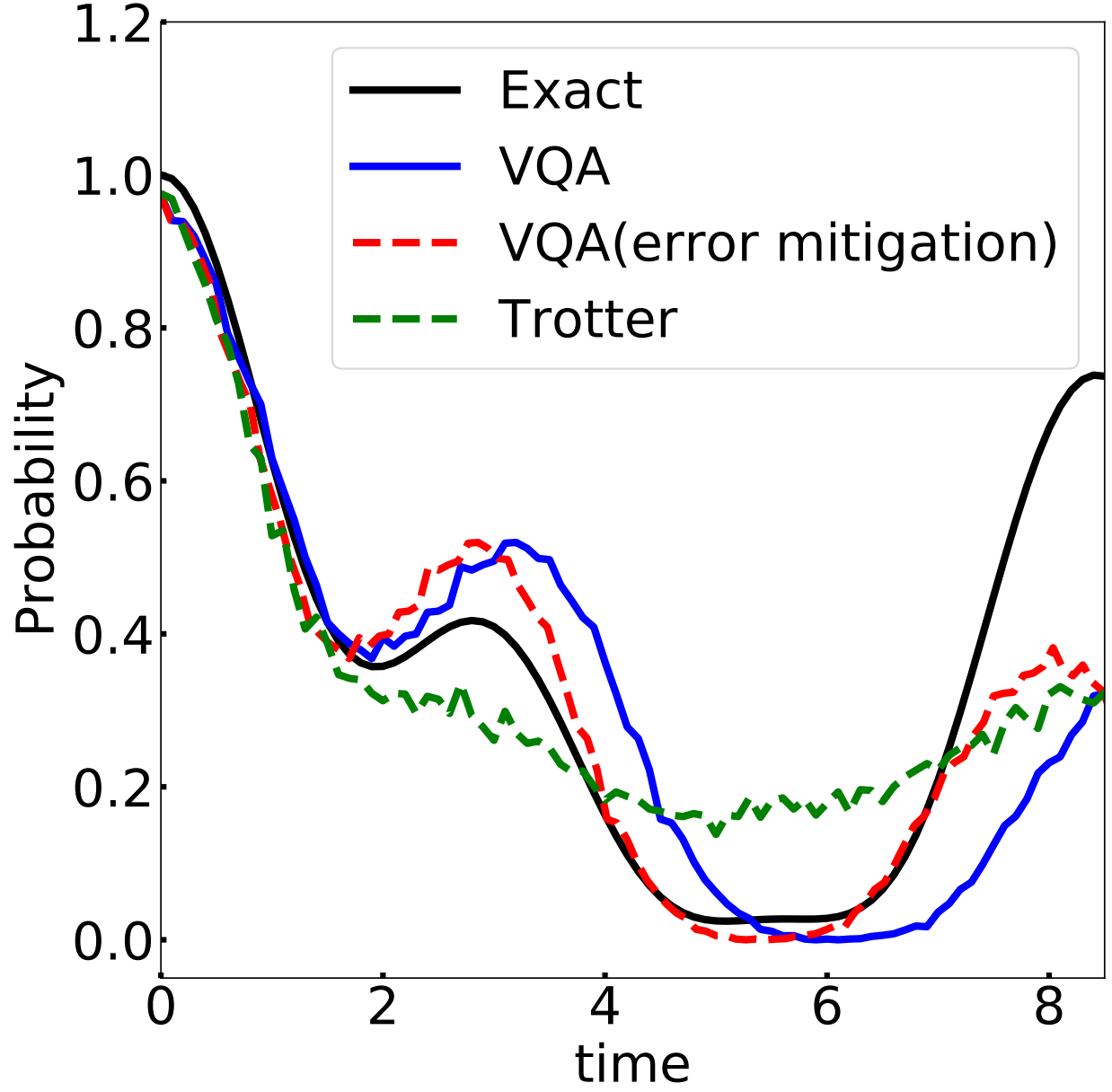
5

FIG. 9: Dynamics of a TFI model obtained from exact diagonalization (black), VQA (blue), VQA with error mitigation (red dashed), and Trotter algorithm (green dashed).

[1] Abraham, H. *et al.* Qiskit: An Open-source Framework for Quantum Computing (2019).